Disorder and its impact on mobility of undoped GaN

Robert A. Makin*

Western Michigan University,1903 W. Michigan Ave, Kalamazoo, Michigan 49008, USA

Andrew Messecar

Western Michigan University, 1903 W. Michigan Ave, Kalamazoo, Michigan 49008, USA

Steven M. Durbin

Western Michigan University, 1903 W. Michigan Ave, Kalamazoo, Michigan 49008, USA and

Present Address: University of Hawaii at Manoa, 2540 Dole Street, Honolulu, Hawaii 96822, USA

(Dated: November 11, 2024)

Abstract

While it is widely appreciated that disorder is intricately related to observed sample-to-sample variation in property values, outside of very specialized cases, analysis is often qualitative in nature. One well-understood quantitative approach is based on the 1930s work of Bragg and Williams, who established an order parameter S which ranges from unity in the case of a perfectly-ordered structure, to zero in the case of a completely randomized lattice. Here, we demonstrate that this order parameter is directly related to charge carrier mobility in undoped GaN. Extrapolating experimental points yields a value of 1640 cm^2/Vs for the maximum room temperature mobility in stoichiometric material, with higher values potentially accessible for Ga-rich material. Additionally, we present a model for observed trends in carrier concentration based on the occurrence of distinct structural motifs, which underpin S. The result is an alternative perspective for the interplay between lattice structure and charge carriers that enables a predictive model for tuning mobility and carrier concentration in undoped material.

* Corresponding author: robert.makin@wmich.edu

Structural disorder impacts a wide range of semiconductor properties including the band gap and the dynamics of charge carrier transport. However, despite its importance, the full extent of the effect on sample-specific attributes is not well understood. From the experimental side, this is often due to a qualitative approach to characterizing disorder in samples, which yields largely general trends. From a theoretical perspective, atomic-level disorder can pose challenges due to the complexity of accurately capturing the impact of randomness within a lattice structure because of prohibitively large lattices that are not computationally feasible. Additionally, disorder is often viewed as detrimental, and as such, is typically the target of minimization efforts at the sample level —limiting the degrees of disorder available for study in a particular material.

One method for quantifying the degree of disorder in a semiconductor is through the Bragg-Williams parameter, S, which measures the degree of structural disorder in a lattice arising from antisite defects [1–3]. We note that while the Bragg-Williams order parameter was developed using binary alloys, it applies without loss of generality to any lattice-based material with one or more constituents [4, 5]. For a given sample of a binary material with elements A and B, $S = r_A + r_B - 1$, where r_A is the fraction of A atoms occupying A lattice sites and r_B is the fraction of B atoms occupying B lattice sites [6]. An ordered lattice, where each atom is on its expected lattice site, corresponds to $S = 1$; this can only occur when there are equal percentages of the constitutive elements of the material, i.e. $x = 0.5$, where x describes the proportion of the various constituents in the material. A completely disordered lattice, corresponding to atoms of each element in the material randomly distributed across the lattice sites, yields $S = 0$. We note that this model can be extended beyond antisite defects to include other types of defects [7], which may also be present in non-stoichiometric layers.

In addition to measuring the degree of disorder in lattices, this framework can also be used to predict relationships between S and material properties. For example, it can be shown that for properties dominated by pair-wise interaction, the value of property $P(x, S)$ is given by [8, 9]

$$P(x, S) = [P(0.5, 1) - P(x, 0)]S^2 + P(x, 0) \tag{1}$$

Consequently, for any property satisfying the necessary interaction conditions, we expect a linear relationship between the property and S^2 for a fixed composition x.

S also provides a pathway to physically understanding the relationship between disorder

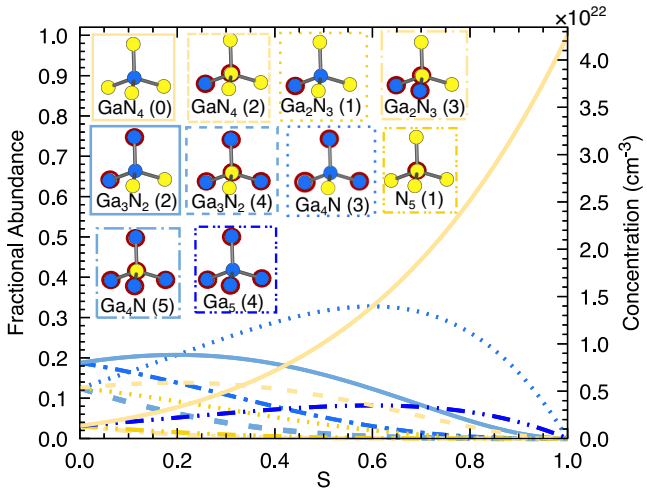

Figure 1. The fractional abundance of each of the 10 possible structural motifs that can occur in GaN as a function of S, at a composition of Ga:N of 1:1. *Inset*: The graphical representation of the motifs, with Ga atoms represented by blue circles and N atoms with yellow; atoms on the incorrect site are highlighted with a red circle. Thus, GaN_4 (0) denotes the basis or fundamental motif, which is the only motif present in samples with $S = 1$. The number in parentheses represents the number of antisite defects characterizing the motif.

and material properties through the lens of structural motifs, which is one means of describing the nearest-neighbor environment of an atom in a material. For a given material system, a set of structural motifs can be defined to account for all possible nearest-neighbor environments that may occur, and the probability of occurrence of each motif can be expressed as a function of S, as illustrated in Fig. 1 for the set of motifs that apply to GaN. In a perfectly ordered ($S = 1$) sample, there is only one set of motifs—the basis motif(s); as varying degrees of disorder are introduced, either by antisite defects or changes in composition, other motif types begin to occur in specific amounts dictated by S. These structural motifs provide a means for physically understanding the effect of disorder on material properties through the impact that differing percentages of each motif type will have on material properties.

In this report, we describe the application of such an approach to measuring structural disorder of undoped GaN samples in order to investigate the relationships between S and both the mobility and carrier concentration, and to provide a possible explanation of observed trends using the set of antisite disorder structural motifs.

GaN films were grown via plasma-assisted molecular beam epitaxy (PAMBE) in a modi-

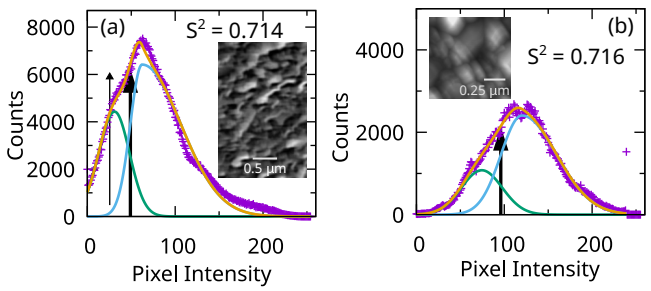

Figure 2. Examples of S measurement using SEM and AFM images, with fitted pixel intensity histograms of an (a) SEM image and (b) AFM image of a PAMBE-grown GaN sample. The light blue curve is the fitted curve for the pixel intensities associated with ordered regions of the sample, and the green curve is the fitted curve for the pixel intensities associated with the disordered regions of the sample. For the SEM and AFM images, the determined threshold and S^2 values were 49 pixels, 0.714 and 96 pixels, 0.716, respectively.

fied 430 Perkin-Elmer system with a base pressure of 5×10^{-11} Torr. Ga flux was provided by an e-Science 85 cm^3 thermal effusion cell. Active nitrogen was provided from an Oxford Applied Research HD-25 RF plasma source and substrates included ytrria-stabilized zirconium, GaN templates, and sapphire. Additionally, we have analyzed published data for undoped GaN films grown by metalorganic vapor phase epitaxy [10], PAMBE [11–18], metalorganic chemical vapor deposition [19–23], chemical co-precipitation [24], electron cyclotron resonance PAMBE [25, 26], sputtering [27], hydride vapor phase epitaxy [28], and reactive closed space sublimation [29].

S can be measured through a variety of different experimental techniques, including x-ray diffraction [6], reflection high energy electron diffraction (RHEED), Raman spectroscopy and electron microscopy [8, 9]. For this study, scanning electron microscopy (SEM) was primarily employed to measure S values; an example of the S measurement process is shown in Fig. 2a. Additionally, some S^2 values were obtained from atomic force microscopy, to which we have recently extended the S^2 measurement methodology; the process is similar to measuring S from SEM. The pixel intensity histogram of the AFM image is fitted with two curves, one corresponding to ordered regions and the other due to disordered regions of the sample; an example analysis for an AFM image of a GaN sample is shown in Fig. 2b. This methodology has proven robust and has excellent agreement with S measured from SEM images where both AFM and SEM measurements are available for a sample. While

both SEM and AFM are surface sensitive, we have previously shown that surface sensitive techniques (e.g. RHEED) provide robust measurements of the S-value for a sample in good agreement with techniques that are not surface-limited, such as x-ray diffraction and Raman spectroscopy [8, 9].

All mobilities of samples measured in this study are room-temperature (RT) Hall effect mobilities. To assist in identifying linear trends between S and the mobility, we consider the general mobility equation $\mu = et_c/m^*$, where e is the elementary charge, t_c is the average time between collisions, and m^* is the effective mass of the charge carrier. This equation holds for both electrons and holes, with the difference being that holes will have a negative effective mass and thus a negative mobility. For the purposes of this discussion, we quote values for hole mobilities as negative and electron mobilities as positive.

It can be shown that the effective mass tensor is strongly dependent upon the charge distribution within the lattice. Starting from the perturbation approach for the effective mass tensor, we include a term for the lattice potential, $U(k+q)$ in the expansion for H_{k+q}, $H_{q+k} = \frac{\hbar^2}{2m}(\frac{1}{i}\nabla + k + q)^2 + U(k+q)$. Performing a Taylor series expansion for the lattice potential and keeping only linear and quadratic terms, we may write $H_{q+k} = H_k + \frac{\hbar^2}{2m}\mathbf{q}\cdot(\frac{1}{i}\nabla + \mathbf{k}) + \frac{\hbar^2}{2m}q^2 + \nabla U\cdot\mathbf{q} + \mathbf{q}^T H_f \mathbf{q}$. This, along with using the Poisson equation in k-space to represent the lattice potential as charge density $U(\mathbf{k}) = \frac{\rho(\mathbf{k})}{k^2\epsilon_r\epsilon_0}$, leads to the following expression for the inverse effective mass tensor:

$$\frac{\partial^2\epsilon_n(\mathbf{k})}{\partial k_i \partial k_j} = \frac{\hbar^2}{m}\delta_{ij} + \frac{\partial^2(\frac{p(\mathbf{k})}{k^2\epsilon_r\epsilon_0})}{\partial k_i \partial k_j} + (\frac{\hbar^2}{m})^2 \sum_{n\neq n}\Bigg(\frac{\langle n\mathbf{k}|\frac{1}{i}\nabla_i + \frac{\partial\frac{p(\mathbf{k})}{k^2\epsilon_r\epsilon_0}}{\partial k_i}|n'k\rangle\langle n'\mathbf{k}|\frac{1}{i}\nabla_j + \frac{\partial\frac{p(\mathbf{k})}{k^2\epsilon_r\epsilon_0}}{\partial k_j}|n\mathbf{k}\rangle}{\epsilon_n(\mathbf{k}) - \epsilon'_n(\mathbf{k})} + \frac{\langle n\mathbf{k}|\frac{1}{i}\nabla_j + \frac{\partial\frac{p(\mathbf{k})}{k^2\epsilon_r\epsilon_0}}{\partial k_j}|n'\mathbf{k}\rangle\langle n'\mathbf{k}|\frac{1}{i}\nabla_i + \frac{\partial\frac{p(\mathbf{k})}{k^2\epsilon_r\epsilon_0}}{\partial k_i}|n\mathbf{k}\rangle}{\epsilon_n(\mathbf{k}) - \epsilon'_n(\mathbf{k})}\Bigg)$$

Thus, given the dependence of $\frac{\partial^2\epsilon_n(\mathbf{k})}{\partial k_i \partial k_j}$ on $p(k)$, the effective mass will be inversely proportional to the charge distribution on the lattice.

Figure 3a shows the experimental relationship between Hall effect mobility and measured S^2 for a set of 49 GaN samples representing 5 different Ga:N ratios. There is a separate linear trend with a different slope and intercept for each composition; however, all linear trends share the same $S = 1$ point. This endpoint, with a mobility of -728 cm^2/(Vs) determined by

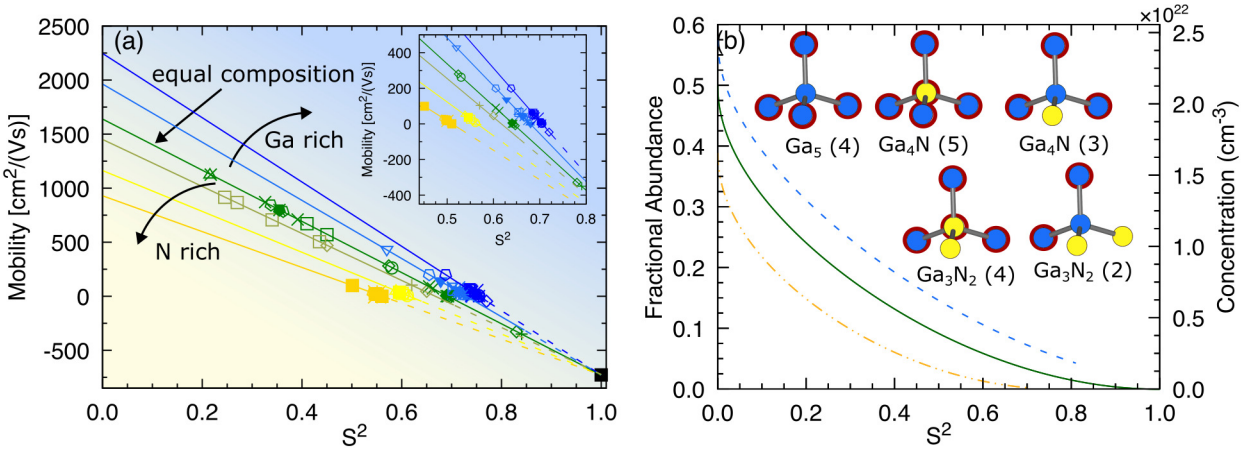

Figure 3. a) Room temperature mobility of GaN as a function of S^2 for 5 different compositions: two N-rich compositions (yellow), an equal composition of N and Ga (green), and two Ga-rich compositions (blue). The fitted linear trends extrapolate to the same value at $S = 1$, (black square). The dashed portions of the linear fits represent S^2 values not accessible for those compositions. Inset highlights points clustered in the upper range of S^2 values. The open points represent films analyzed from the literature: orange, yellow and blue squares [20]; yellow triangles [29]; yellow and blue circles [27]; green and blue diamonds [15]; green pentagons [13]; green and light blue 'x's [12]; green triangles [28]; green circles [11]; light blue and blue triangle [19]; light blue and blue inverted triangles [10]; light blue and blue pentagon [14]; blue plus sign [25]; yellow and blue asterisks [30]; green and dark yellow plus signs [31, 32]; green and dark yellow squares [17]; green 'x's [18]; green, light and dark blue asterisks [26]; dark blue 'x' [22]; light blue diamond [24]; light blue square [16]; light and dark yellow pentagon [21]; green solid pentagon [23]. Data organized by reference is available online [33]. b) The total fractional abundance (and concentration) of Ga-rich motifs in GaN as a function of S^2 for three different compositions: an N-rich composition (dashed and dotted yellow), an equal composition of N and Ga (solid green), and a Ga-rich composition (dashed blue). Inset are the set of Ga-rich motifs. We note it is somewhat of an open question as to what an existence range might be for non-stoichiometric compounds, as pointed out by Libowitz [34], who also noted that wide compositional variations can occur at elevated temperatures—which generally leads to a reduction in S.

extrapolation from the three fitted linear trend lines, provides an explanation for reports of p-type conductivity in highly ordered undoped GaN (zero antisite defects and precisely 1:1

Ga:N composition), as well as for samples with S^2 values greater than approximately 0.5 to 0.7 for GaN at the off-stoichiometric compositions shown [15, 31, 35]. Overall, the trends demonstrate that with increasing Ga concentration, the mobility of n-type (undoped) GaN increases with increasing disorder, while the mobility of p-type (undoped) GaN increases with decreasing disorder. More specifically, these results indicate it may be possible to increase the mobility of undoped n-type GaN beyond the current highest reported values, which lie between 1100 and 1300 $cm^2/(Vs)$ [13, 28, 36], by decreasing S towards 0; for example in the case of a Ga:N ratio of 1:1 the predicted $S = 0$ mobility from the fitted trend line is 1640 $cm^2/(Vs)$.

The trends for the mobility of undoped GaN follow the changes in structural motif with composition and degree of disorder. With increasing disorder and increasing Ga concentration, the percentage of Ga-rich motifs increases, as shown in Fig. 3b. Ga-rich motifs are positively charged and thus contribute to a reduced effective mass for electrons moving through the material, corresponding to an increased n-type mobility. Conversely, as S^2 increases and the Ga concentration decreases, the percentage of Ga-rich motifs decreases—stated another way, the percentage of N-rich motifs will increase. N-rich motifs are negatively charged; thus, when dominating a sample, they will lead to a negative effective mass for electrons, resulting in p-type conductivity and increasing carrier mobility as the percentage of N-rich motifs present in the sample increases. Trends in carrier transport properties in GaN are commonly attributed to defects more energetically favorable than antisites, such as Ga-vacancies, as determined by first principles calculations for well-ordered GaN [7]. However, while these results for well-ordered GaN can provide useful insights for disordered GaN, well-ordered lattices differ from disordered ones, especially in regard to band structure [37] and by extension the defect properties that are dependent on the Fermi level, conduction band edge, or relative location of the defect energy levels. Thus, the carrier transport properties in disordered GaN represent open questions worth pursuing, and Fig. 3 suggests that both energy and entropy should be considered for disordered GaN.

Another key characteristic of semiconductors closely related to the mobility is the carrier concentration. Figure 4 shows the carrier concentration as a function of S for each of the samples from the 6 compositions of GaN in Fig 3a. While there appears to be no linear relationship between S^2 and the carrier concentration as observed for the mobility, the carrier concentrations do appear to correlate to the percentages of motifs as dictated by x and S.

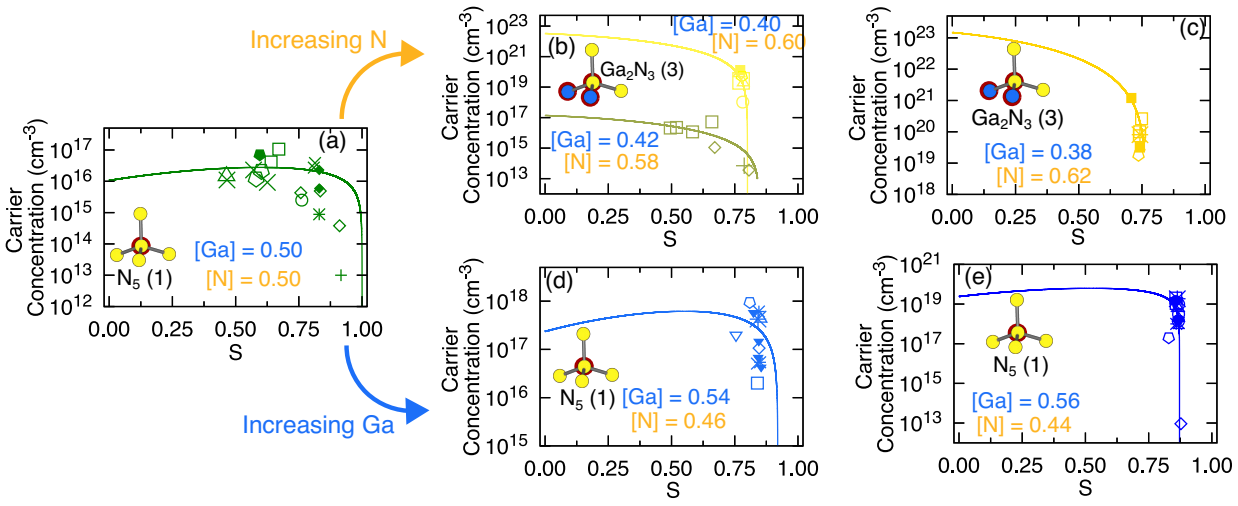

Figure 4. Carrier concentration of GaN samples as a function of S for 5 different compositions: (a) Ga=0.5, N=0.5; (b) Ga=0.4,N=0.6; (c) Ga=0.38, N=0.62; (d)Ga=0.54, N=0.46,(e) Ga=0.56, N=0.44. Also shown is the corresponding motif that best fits the data for the given composition (inset). The open points represent films analyzed from the literature: orange, yellow and blue squares [20]; yellow triangles [29]; yellow and blue circles [27]; green and blue diamonds [15]; green pentagons [13]; green triangles [28]; green and light blue 'x's [12]; green circles [11]; light blue and blue triangle [19]; light blue and blue inverted triangles [10]; light blue and blue pentagon [14]; blue plus sign [25]; yellow and blue asterisks [30]; green and dark yellow plus signs [31, 32], green and dark yellow squares [17], green 'x' [18], green, light and dark blue asterisks [26], dark blue 'x' [22], light blue diamond [24], light blue square [16], light and dark yellow pentagon [21], green solid pentagon [23]. Data organized by reference is available online [33].

To determine which motif or combination of motifs best correlates to the data, each of the 512 possible combinations of the 9 non-basis motifs were fit to the carrier concentrations for each composition (the basis motif was excluded since it has no net charge). The resulting best fits are shown in Figs. 4a-e with the corresponding motif inset in each plot. The best overall fits were selected using standard criteria for a best-subset selection methodology, where the best overall fit among all the possible combinations is the one with the smallest number of variables for which fits with higher number of variables offer no meaningful improvement in the adjusted residual sum of squares value. The trend that emerges from the fits across all the compositions is that the motifs which best fit the experimental data are all N-dominated motifs, and from all the possible combinations of motifs considered,

the best fit was always a single motif and not a combination of motifs. While additional data points across a wider range of S values are needed to provide more robust conclusions, these results suggest that the largest contributors of carriers in undoped GaN are specific N-dominated motifs. At N-heavy compositions (Fig. 4b and c) this motif is $Ga_2N_3(3)$, while for Ga-heavy concentrations as well as compositions with equal amounts of Ga and N (Fig. 4a,d, and e) it is the $N_5(1)$ motif.

These motifs dominate the carrier concentrations at the indicated ranges most likely due to their relative percentages at the respective compositions. $Ga_2N_3(3)$, due to its three antisite constituents—two of which are Ga atoms on N-sites—will be more abundant at higher degrees of disorder and at compositions with higher nitrogen concentrations where the fraction of Ga atoms on the correct lattice sites will be the smallest. Likewise, $N_5(1)$, due to its one nitrogen antisite constituent, is more likely to occur at lower degrees of disorder and at compositions with more Ga, since it requires only 1 N atom to be out of place. However, further study is required to better understand why specific motifs dominant the contributions to the overall carrier concentration.

The mobility of undoped GaN has been experimentally demonstrated to exhibit a linear relationship with S^2, the squared Bragg-Williams order parameter, as expected for a property dominated by pair-wise interactions. Additionally, the carrier concentration was shown to have a direct dependence on the occurrence of specific motifs at given Ga:N ratios. Thus, tuning both the mobility and carrier concentration of undoped GaN through disorder is possible; further, the methodology provides an additional means of determining the full range of achievable mobility values for this semiconductor. However, it is important to keep in mind that while disorder may tune the mobility and carrier concentration of GaN, it will also tune other material properties, such as the band gap, simultaneously. The results also suggest that mobility in general maybe viewed as a pair-wise dominated property and thus other semiconductors may exhibit a linear relationship between charge carrier mobility and S^2.

SUPPLEMENTARY MATERIAL

See the supplementary material for the experimentally observed temperature dependence of S^2 in a GaN sample as well as a comparison of S^2 values calculated from different exper-

imental techniques for 15 different GaN samples.

DATA AVAILABILITY

The data that support the findings of this study are available from the online repository [33].

ACKNOWLEDGMENTS

This work was performed with partial support from the National Science Foundation (DMR-2003581, S.D. and R.M.) and Western Michigan University. Analysis was performed using hardware received through the NVIDIA Academic Hardware grant program (R.M.).

GaN growth was performed by P. Anderson and C. Kendrick with financial support from the MacDiarmid Institute for Advanced Materials and Nanotechnology (S.D.).

---

[1] W. L. Bragg and E. J. Williams, "The effect of thermal agitation on atomic arrangement in alloys," Proceedings of the Royal Society of London. Series A, Containing Papers of a Mathematical and Physical Character **145**, 699–730 (1934).

[2] W. L. Bragg and E. J. Williams, "The effect of thermal agitation on atomic arrangement in alloys II," Proceedings of the Royal Society of London. Series A - Mathematical and Physical Sciences **151**, 540–566 (1935).

[3] E. J. Williams and W. L. Bragg, "The effect of thermal agitation on atomic arrangement in alloys-III," Proceedings of the Royal Society of London. Series A - Mathematical and Physical Sciences **152**, 231–252 (1935).

[4] S. Nakatsuka and Y. Nose, "Order–disorder phenomena and their effects on bandgap in $ZnSnP_2$," The Journal of Physical Chemistry C **121**, 1040–1046 (2017).

[5] S. Francoeur, G. A. Seryogin, S. A. Nikishin, and H. Temkin, "Quantitative determination of the order parameter in epitaxial layers of $ZnSnP_2$," Applied Physics Letters **76**, 2017–2019 (2000).

[6] B. Warren, *X-Ray Diffraction*, Dover Books on Physics (Dover Publications, 2012).

[7] G. Miceli and A. Pasquarello, "Energetics of native point defects in GaN: A density-functional study," Microelectronic Engineering **147**, 51–54 (2015).

[8] R. A. Makin, K. York, S. M. Durbin, and R. J. Reeves, "Revisiting semiconductor band gaps through structural motifs: An Ising model perspective," Physical Review B **102**, 115202 (2020).

[9] R. A. Makin, K. York, S. M. Durbin, N. Senabulya, J. Mathis, R. Clarke, N. Feldberg, P. Miska, C. M. Jones, Z. Deng, L. Williams, E. Kioupakis, and R. J. Reeves, "Alloy-Free Band Gap Tuning across the Visible Spectrum," Physical Review Letters **122**, 256403 (2019).

[10] I. Akasaki, H. Amano, Y. Koide, K. Hiramatsu, and N. Sawaki, "Effects of AIN buffer layer on crystallographic structure and on electrical and optical properties of GaN and $Ga_{1-x}Al_xN$ (0 ¡ x $\leq$ 0.4) films grown on sapphire substrate by MOVPE," Journal of Crystal Growth **98**, 209–219 (1989).

[11] P. Kordoš, M. Morvic, J. Betko, J. M. Van Hove, A. M. Wowchak, and P. P. Chow, "Conductivity and hall effect characterization of highly resistive molecular-beam epitaxial GaN layers," Journal of Applied Physics **88**, 5821–5826 (2000).

[12] N. Fujita, M. Yoshizawa, K. Kushi, H. Sasamoto, A. Kikuchi, and K. Kishino, "Epitaxial growth of GaN with a high growth rate of 1.4μm/h by RF-radical source molecular beam epitaxy," Journal of Crystal Growth **189-190**, 385–389 (1998).

[13] B. Heying, I. Smorchkova, C. Poblenz, C. Elsass, P. Fini, S. Den Baars, U. Mishra, and J. S. Speck, "Optimization of the surface morphologies and electron mobilities in GaN grown by plasma-assisted molecular beam epitaxy," Applied Physics Letters **77**, 2885–2887 (2000).

[14] A. Mizerov, V. Jmerik, V. Kaibyshev, T. Komissarova, S. Masalov, A. Sitnikova, and S. Ivanov, "Growth control of n-polar GaN in plasma-assisted molecular beam epitaxy," Acta Physica Polonica A **114**, 1253–1258 (2008).

[15] S. Buczkowski, *Nucleation and Growth of GaN on Sapphire by MBE*, Ph.D. thesis, West Virginia University (1996).

[16] C. Heinlein, J. K. Grepstad, H. Riechert, and R. M. Averbeck, "Radio frequency plasma nitridation of c-plane sapphire; influence on properties of gan grown by molecular beam epitaxy," Materials Science and Engineering B-advanced Functional Solid-state Materials **58**, 270–273 (1999).

[17] G. Koblmüller, F. Reurings, F. Tuomisto, and J. S. Speck, "Influence of Ga/N ratio on

morphology, vacancies, and electrical transport in GaN grown by molecular beam epitaxy at high temperature," Applied Physics Letters **97**, 191915 (2010).

[18] G. Koblmüller, F. Wu, T. Mates, J. S. Speck, S. Fernández-Garrido, and E. Calleja, "High electron mobility GaN grown under N-rich conditions by plasma-assisted molecular beam epitaxy," Applied Physics Letters **91**, 221905 (2007).

[19] S.-E. Park, W. Seok Han, H. Gyoo Lee, and B. O, "Effect of native defects on electrical and optical properties of undoped polycrystalline GaN," Journal of Crystal Growth **253**, 107–111 (2003).

[20] C. J. Sun, P. Kung, A. Saxler, H. Ohsato, E. Bigan, M. Razeghi, and D. K. Gaskill, "Thermal stability of GaN thin films grown on (0001) Al_2O_3, (0112) Al_2O_3 and (0001)Si 6H-SiC substrates," Journal of Applied Physics **76**, 236–241 (1994).

[21] . Sugianto, R. Sani, P. Arifin, M. Budiman, and M. Barmawi, "Growth of gan film on a-plane sapphire substrates by plasma-assisted mocvd," Journal of Crystal Growth **221**, 311–315 (2000), proc Tenth Int Conf Metalorganic Vapor Phase Epitaxy.

[22] V.-T. Rangel-Kuoppa, C. G. Aguilar, and V. Sánchez-Reséndiz, "Structural, optical and electrical study of undoped gan layers obtained by metalorganic chemical vapor deposition on sapphire substrates," Thin Solid Films **519**, 2255–2261 (2011).

[23] K. Kim, C. Oh, W.-H. Lee, K. Lee, G. Yang, C.-H. Hong, E.-K. Suh, K. Lim, H. Lee, and D. Byun, "Comparative analysis of characteristics of si, mg, and undoped gan," Journal of Crystal Growth **210**, 505–510 (2000).

[24] M. Gopalakrishnan, V. Purushothaman, V. Ramakrishnan, G. M. Bhalerao, and K. Jeganathan, "The effect of nitridation temperature on the structural, optical and electrical properties of gan nanoparticles," CrystEngComm **16**, 3584–3591 (2014).

[25] C. R. Eddy, T. D. Moustakas, and J. Scanlon, "Growth of gallium nitride thin films by electron cyclotron resonance microwave plasma-assisted molecular beam epitaxy," Journal of Applied Physics **73**, 448–455 (1993).

[26] R. J. Molnar and T. D. Moustakas, "Growth of gallium nitride by electron-cyclotron resonance plasma-assisted molecular-beam epitaxy: The role of charged species," Journal of Applied Physics **76**, 4587–4595 (1994).

[27] C.-C. Li and D.-H. Kuo, "Effects of growth temperature on electrical and structural properties of sputtered GaN films with a cermet target," Journal of Materials Science: Materials in

Electronics **25**, 1404–1409 (2014).

[28] F. Yun, M. Reshchikov, K. Jones, P. Visconti, H. Morkoç, S. Park, and K. Lee, "Electrical, structural, and optical characterization of free-standing GaN template grown by hydride vapor phase epitaxy," Solid-State Electronics **44**, 2225–2232 (2000).

[29] Y. Watanabe and M. Sano, "Low-temperature growth of GaN epitaxial layers with buffer layers by reactive close-spaced method," Japanese Journal of Applied Physics **42**, 384 (2003).

[30] J.-M. Myoung, *Growth kinetics of GaN and effects of flux ratio and growth temperature on properties of undoped and Mg-doped GaN films grown by PAMBE*, Ph.D. thesis, University of Illinois at Urbana-Champaign (1998).

[31] D. J. As, D. Schikora, A. Greiner, M. Lübbers, J. Mimkes, and K. Lischka, "*p*- and *n*-type cubic GaN epilayers on GaAs," Physical Review B **54**, R11118–R11121 (1996).

[32] D. Schikora, M. Hankeln, D. J. As, K. Lischka, T. Litz, A. Waag, T. Buhrow, and F. Henneberger, "Epitaxial growth and optical transitions of cubic GaN films," Physical Review B **54**, R8381–R8384 (1996).

[33] R. Makin, M. A., and S. Durbin, "Data repository for disorder and its impact on mobility of undoped GaN," (2023), `https://doi.org/10.5281/zenodo.8133233`.

[34] G. G. Libowitz, "Nonstoichiometry in chemical compounds," Progress in Solid State Chemistry **2**, 216–264 (1965).

[35] M. Rubin, N. Newman, J. S. Chan, T. C. Fu, and J. T. Ross, "p-type gallium nitride by reactive ion-beam molecular beam epitaxy with ion implantation, diffusion, or coevaporation of Mg," Applied Physics Letters **64**, 64–66 (1994).

[36] D. C. Look and J. R. Sizelove, "Predicted maximum mobility in bulk GaN," Applied Physics Letters **79**, 1133–1135 (2001).

[37] D. B. Laks, S.-H. Wei, and A. Zunger, "Evolution of alloy properties with long-range order," Phys. Rev. Lett. **69**, 3766–3769 (1992).